Master's Thesis

The cheerio mechanosensory region fine-tunes *Drosophila* cellularization

Mikko Hakanen

University of Jyväskylä

Department of Biological and Environmental Science

14 May 2024

UNIVERSITY OF JYVÄSKYLÄ, Faculty of Mathematics and Science
Department of Biological and Environmental Science
Master's Degree Programme in Cell and Molecular Biology
Hakanen, Mikko E.W. — The cheerio mechanosensory region fine-tunes *Drosophila* cellularization
MSci Thesis — 28 p., 3 appendices (4 s.)
Supervisors: — Professor Jari Ylänne and MSc Riku Korkiamäki
Tarkastajat: — PhD Simon Leclerc and PhD Visa Ruokolainen
May 2024

Keywords: Actin crosslinker, Actomyosin, Filamin

Cellularization, a process in the *Drosophila melanogaster's* embryo stage requires actomyosin polymerization and contraction for membrane invagination and formation of individual cells after multiple mitosis. To accomplish this cellularization utilizes different actin crosslinkers to control the shape and size of actomyosin rings. One of these actin crosslinkers is cheerio, an orthologue of filamin, which contains a mechanosensory region with two masked protein interaction sites in its C-terminal. The role of this region in cellularization is not yet clear. Cellularization from three different fly lineages, which differed in the ease of access to their protein interaction sites, was imaged from living embryos. Confocal microscopy stacks were taken with 3-minute intervals and the localization of cheerio at the actomyosin ring was followed with a GFP tag. The genotype with the least restriction to its protein interaction site separated itself from other genotypes by its perimeter and circularity values and by being localized differently. It obtained larger perimeter length values throughout the cellularization process and decreased in circularity values through the late cellularization. This genotype also had most of its cheerio localized away from the actomyosin rings. These results suggest that the cheerio mechanosensory region affect the actomyosin rings during cellularization, either directly by altering their conformation and contraction, or indirectly by localizing cheerio away from the rings and letting the process complete without the crosslinker's influence. The results are also in accordance with previous filamin studies suggesting that the mechanosensory region is responsible for the filamins attachment to membrane through transmembrane protein interaction. Based on this the mechanosensory region of cheerio seems to also control the localization of cheerio.

JYVÄSKYLÄN YLIOPISTO, Matemaattis-luonnontieteellinen tiedekunta
Bio- ja ympäristötieteiden laitos
Solu- ja molekyylibiologian maisteriohjelma

Hakanen,	Cheerio mekanosensorinen alue hienosäätää
Mikko E.W.	*Drosophilan* soluuntumista
Pro gradu tutkielma:	28 s., 3 liitettä (4 s.)
Työn ohjaajat:	Professori Jari Ylänne ja MSc Riku Korkiamäki
Tarkastajat:	FT Simon Leclerc ja FT Visa Ruokolainen
Toukokuu 2024	

Hakusanat: Aktiinisäikeitä yhteenliittävä proteiini, Aktomyosiini, Filamiini

Drosophila melanogasterin alkiovaiheen aikana tapahtuvassa soluuntumisessa on mukana useita eri aktiinisäikeitä yhteenliittäviä proteiineja, jotka kontrolloivat aktomyosiinirenkaan muotoa ja kokoa. Filamiinin ortologi cheerio on yksi näistä proteiineista. Sen karboksipäässä on mekanosensorinen alue, joka sisältää kaksi peitettyä proteiinin vuorovaikutuspaikkaa. Tämän alueen rooli soluuntumisessa ei ole vielä täysin selvillä. Kokeessa käytettiin kolmea eri kärpäslinjaa, jotka vaihtelivat proteiinien vuorovaikutuspaikkojen saavutettavuuden helppoudessa. Alkion soluuntumista kuvattiin elävistä alkioista. Konfokaali mikroskoopi pinoja otettiin 3 minuutin välein ja cheerion sijoittumista sekä aktomyosiinirengasta soluuntumisen aikana seurattiin GFP-tunnisteen avulla. Linja, jonka proteiinin vuorovaikutusalue oli vähiten peitetty, erottui muista linjoista renkaan kehän pituuden ja pyöreyden, sekä cheerion sijoittumisen suhteen. Tämän linjan renkaiden kehän pituus pysyi muita linjoja suurempana koko soluuntumisen ajan, kun taas linjan renkaiden pyöreys laski myöhäisen soluuntumisen aikana. Iso osa cheerio proteiineista tämän linjan soluuntumisessa sijoittuivat pois aktiinimyosiinirenkaiden luota. Tulosten perusteella vaikuttaa siltä, että cheerion mekanosensoriselle alueelle on jonkinlainen vaikutus aktomyosiinirenkaaseen, joko suoraan tai epäsuorasti. Suoraan vaikuttamalla renkaiden muotoon ja supistumiseen tai epäsuorasti muiden vuorovaikutusten kanssa. Tulokset sopivat yhteen aikaisempiin tutkimustuloksiin, joiden mukaan mekanosensorinen alue on vastuussa filamiinin interaktiosta solukalvon proteiinien kanssa ja näin myös tämän kiinnittymisestä solukalvoon. Tätä kautta cheerion mekanosensorinen alue näyttää myös kontrolloivan cheerion lokalisaatiota.

TABLE OF CONTENTS

1 INTRODUCTION 1
1.1 Actin and its crosslinker Filamin 1
1.2 Cellularization – a bridge from uni- to multicellular form 2
1.3 Numerous factors take part in cellularization 3
1.4 The events of cellularization 4
1.5 Study goals and hypotheses 6

2 MATERIALS AND METHODS 7
2.1 Materials 7
2.2 Methods 8
2.2.1 Preparation for imaging 8
2.2.2 Confocal microscope 8
2.2.3 Image analysis 9
2.2.4 Statistical analysis 10

3 RESULTS 10
3.1 Filamin in the cellularization front is less localized around the nuclei in the OPEN genotype compared to other genotypes 10
3.2 The filamin rings of the OPEN genotype separated themselves with their perimeter length and circularity compared to other two genotypes 11

4 DISCUSSION 14
4.1 OPEN cheerio mutant affected the distribution and the dynamics of the actomyosin ring 14
4.2 CLOSED cheerio mutant did not have effect on either the distribution or the dynamics of the actomyosin ring 16
4.3 Limitations and future prospects 16

5 CONCLUSIONS 18

ACKNOWLEDGEMENTS 19

REFERENCES 20

APPENDIX 1. MACROS & SCRIPTS 25

APPENDIX 2. COLLECTION OF TOPDOWN AND SIDE IMAGES OF THE THREE GENOTYPES 27

APPENDIX 3. PERIMETER LENGTH, CIRCULARITY AND DEPTH OF THE CELLULARIZATION FRONT PER TIME 28

TERMS AND ABBREVIATIONS

Terms

Actin crosslinker	Protein that affects actomyosin contraction and architecture
Actomyosin ring	Ring structure formed by actin and myosin-II
Cellularization	Process during *Drosophila* embryo development
Cheerio	*Drosophila* orthologue of Filamin
Filamin	Actin crosslinking class of protein

Abbreviations

GFP	green fluorescent protein
MSR	mechanosensory region
WT	wild type

1 INTRODUCTION

1.1 Actin and its crosslinker Filamin

Actin cytoskeleton, formed from F-actin filaments, is located beneath the cell membrane. It is needed to upkeep or alter cell shape and is responsible for cell motility. Individual actin filaments connect to specific domains at the plasma membrane (Levayer and Lecuit 2012, Murrell et al. 2015). The actin contraction requires molecular motor, such as myosin-II, activity (Agarwal and Zaide-Bar 2019). Myosin-II itself needs to be phosphorylated to become active, bind to actin filaments and get them to slide against each other generating contractions (Pollard and Wu 2010, Reymann et al. 2012, Blanchoin et al. 2014, Chugh et al. 2017, Koenderink and Paluch 2018). This happens via actin cytoskeleton interactions with cell membrane and the many proteins located in it (Sokol et al. 1999). For actin cytoskeleton to be able to affect the cell membrane properties, it itself is controlled by various set of proteins called actin binding proteins (Zhou et al. 2009).

One type of actin binding proteins is called crosslinkers. These proteins connect actins to each other and generate various actin networks that differ in their architecture and ability to contract (Svitkina and Borisy 1999, Laporte et al. 2012, Blanchoin et al. 2014, Chugh et al. 2017, Koenderink and Paluch 2018). Studies have shown that crosslinker concentration levels change the actin network's contraction properties. Lower concentration can lead to non-contractile actin filaments, while higher concentration leads to filamin contraction. Increasing the concentration above certain level leads to actin filaments becoming unable to contract (Bendix et al. 2008, Ennomani et al. 2016, Belmonte et al. 2017). Crosslinkers with lower molecular weight seem to facilitate the formation of actin bundles, while crosslinkers with high molecular weight more often than not lead to mesh-like networks with low contractile properties (Schmoller et al. 2009).

Filamin is a large dimeric actin crosslinker with a large molecular weight and three mammalian isoforms (Hartwig and Stossel 1975, Wang et al. 1975). Filamin can bind to actin in non-muscle cells and facilitates the reorganization of the actin network into a dynamic three-dimensional structure (Hartwig and Stossel 1975, Stendahl et al. 1980, Weihing et al. 1985, Gorlin et al. 1990). They also attach these actin filaments to the plasma membrane through transmembrane receptors and ion channels (Stossel et al. 2001). There is evidence that actin to filamin ratio affects the filamin's actin binding activity (Hartwig and Stossel 1981). These crosslinkers are versatile when it comes to their interaction potential as in addition to actin they are able to interact with up to 70 cellular proteins which vary in their functional properties (Zhou et al. 2007). These include transmembrane receptors and signaling molecules (Zhou et al. 2007).

This makes filamins exceptionally versatile signaling scaffolds (Feng et al. 2004). Filamins are also likely important in mammalian cell movement (Stossel et al. 2001).

Cheerio is a *Drosophila melanogaster* ortholog of filamin (Li et al. 1999, Sokol and Cooley 1999). It has a V-like shape with actin binding sites (ABD) located at the N-terminal's two ends where the rod-like domains are farthest from each other (Huelsmann et al. 2016). The other end, called C-terminal, where the rod like domains is connected has two mechanosensory regions (MSR) (Huelsmann et al. 2016). The MSR is regulated through pulling forces generated by the movement of the attached actin filaments (Huelsmann et al. 2016). While the MSR is unaffected by pulling forces it is in closed conformation with its two protein interaction sites masked by the neighboring sequences (Huelsmann et al. 2016). Pulling forces of 2-5 pN pull open the MSR revealing these two sites and enabling potential interactions with available proteins (Rognoni et al. 2012, Huelsmann et al. 2016).

Cheerio is active during the fly's early development during a phase called cellularization (Li et al. 1999, Sokol and Cooley 1999, Krueger et al. 2019). Cheerio organizes actins filaments into thick bundles that form into hexagonal patterns (Krueger et al. 2019). It functions similarly to other actin crosslinker active during cellularization called bottleneck and the two crosslinkers work synergistically (Krueger et al. 2019). Like human filamin, cheerio is also a likely phosphoprotein able to activate myosin-2 and through this actin filament movement (Ohta and Hartwig 1996). It is however not clear which kinases interact with filamin. Likewise, how cheerio binds to the plasma membrane is unknown although one potential binding-partner is the glycoprotein D-mucin (Kramerov et al. 1997).

The role of the cheerio MSR in cellularization or even the filamin MSR role in its activities is not thoroughly elucidated. Two cheerio mutations were created, with one, having unmasked conformation and therefore higher binding activity in the MSR protein interaction sites (OPEN) and the other mutation having a higher force threshold required to unmask the protein interaction sites (CLOSED) (Huelsmann et al. 2016). It was found that the OPEN mutation was less dynamic compared to wild type (WT) and seemed to be more tightly connected to the plasma membrane (Huelsmann et al. 2016). The CLOSED mutation on the other hand showed greater dynamics (Huelsmann et al. 2016). OPEN MSR recovered slower compared to WT while CLOSED recovered faster and seemed to be influenced more by other filamin regions like the ABD (Huelsmann et al. 2016). It seems that the cheerio C-terminal is more active in protein dynamics and in connecting it to the membrane while N-terminal and the ABD has no notable role in localization, but only in actin binding (Huelsmann et al. 2016).

1.2 Cellularization – a bridge from uni- to multicellular form

During *Drosophila* melanogaster embryo development, the first cells are formed in a process called cellularization that requires rapid and precise cytokinesis. During this process numerous individual nuclei, under the fertilized embryo

membrane, have a new membrane grow and envelop them (Sokac et al. 2023). The end result is a multicellular sheet of mononuclear epithelial cells (Figure 1 A3), and the embryo is ready to continue to develop into the larval stage (Sokac et al. 2023). Before the cellularization phase itself, the fertilized embryo's nuclei begin to divide but cell division does not occur. This is why these cycles are often called nuclear cycles. The nuclei continue to divide nine times in the center of the embryo (Figure 1 A1). Between the ninth and tenth divisions these nuclei move to the periphery under the embryo's plasma membrane and continue to divide (Figure 1 A2) (Foe and Alberts 1983). By the 14th division there are around 6000 cells situated evenly just under the cell membrane of the embryo and the cellularization itself can begin (Foe and Alberts 1983, Lecuit and Wieschaus 2000). During cellularization the embryo's cell membrane starts to invaginate inward towards the center of the embryo and simultaneously form furrows around every nucleus anchored under the cell membrane. The leading edge of these furrows is called cellularization front. The outer rings located on the front that surround the nuclei are formed by actomyosin, which change the ring shape and size during cellularization (Schejter and Wieschaus 1993). Cellularization takes about one hour and ends with the furrows closing under the nuclei engulfing them and forming a sheet of mononuclear cells around the embryo (Sokac et al. 2023). After cellularization the newly formed cells start to build gastrula's multi-layered tissues as the embryo develops towards a hatching larva (Sokac et al. 2023).

Cellularization is a dynamic process, that can be divided into different phases, for example based on the rate of invagination or the perimeter of the actomyosin rings. The phases based on the ring conformation and size include assembly phase, hexagonal phase, ring phase and the fast constriction phase (Xue and Sokac 2016, Krueger et al. 2019). The phases based on front's furrowing speed include the slow- and the fast-furrowing phases both taking about 30 minutes to complete (Sokac et al. 2023). During the former the rings go through their assembly and hexagonal phases and the start of the ring phase, while the latter begins concurrently with the ring phase and continues throughout the fast constriction phase (Krueger et al. 2019).

1.3 Numerous factors take part in cellularization

Cellularization is an abnormally rapid form of cytokinesis that, in order to be completed correctly, requires proper timing and interplay of various phases. This in turn requires correct F-actin dynamics and architecture as well as correct motor activity of myosin-2, both of which are coordinated through membrane trafficking and remodeling mechanisms (Sokac et al. 2023). The correct composition of components in each part of the furrow is also vital. These compartments are apical, subapical, lateral and basal. Each compartment is located further down the furrows with the last one, basal, being located at furrow tips. The compartments include components like crosslinkers and F-actin nucleators among others (Chugh and Paluch 2018). These components are embedded in an F-actin meshwork called the actin cortex that surrounds the

furrowing plasma membrane (Chugh and Paluch 2018, Kelkar et al. 2020). Cytoplasm flow called 'cortical flow' transfers myosin-2 (He et al. 2016). Endocytosis, controlled by number of proteins like F-actins, is used to ensure the correct components composition at basal level and therefore it regulates the invagination of the furrow and actomyosin contraction that takes place at the cellularization front (Sokac and Wieschaus 2008, Lee and Harris 2013, Liu et al. 2015, Su et al. 2013, Yan et al. 2013).

There are three somewhat distinct membrane trafficking routes used during cellularization, that differ in their timing, function and the path they take (Sokac and Wieschaus 2008, Lee and Harris 2013, Su et al. 2013, Yan et al. 2013, Liu et al. 2015). These routes are not, however, completely unique as the content of their cargo may overlap. At the beginning of cellularization one route is used to build the furrow's F-actin cortex (Cao et al. 2008). In addition to F-actin, the cargo trafficked by this route includes actin regulators (Cao et al. 2008, Holly et al. 2015). The second route is responsible for trafficking the membrane stored at the apical microvilli, which is used to build the growing furrows (Figard et al. 2013, Figard et al. 2016). These two routes are active during the slow furrowing phase (Sokac et al. 2023). The third route, active during the fast-furrowing phase, likely traffics membrane and components needed during the late stages of cellularization (Lecuit and Wieschaus 2000, Lecuit 2004, Murthy et al. 2010, Mavor et al. 2016).

At basal level, perhaps more than any other cellularization site, having the correct components at correct levels at the correct time is important This is because this site is not only responsible for building the furrows and the actomyosin rings but also closing them when proper depth has been achieved. Trafficking pathways dependent on Rab11 and recycling endosomes localize numerous important components at the tip of the furrows (Cao et al. 2008, Acharya et al. 2014). Mechanical forces required for furrow invagination and closure of the furrow tips are likely generated by plus-end directed microtubule motors located in the basal compartment instead of myosin-2 contraction (Minestrini et al. 2003, Sommi et al. 2010). The composition at the basal compartment is indirectly controlled by a number of proteins, which are necessary for endocytosis that removes the surplus proteins and membrane (Sokac and Wieschaus 2008, Lee and Harris 2013, Su et al. 2013, Yan et al. 2013, Liu et al. 2015).

1.4 The events of cellularization

The actomyosin rings begin to form before 4 μm front depth (Figure 1 B1) (Krueger et al. 2019, This study). During this 'assembly phase' the actomyosin rings take on undefined shapes (Figure 1 B1', B1''). Myosin-2 is procured to the basal layer by Dunk and Slam gene products through cortical flow and recruitment via RhoGEF2 (Wenzl et al. 2010, He et al. 2016). The latter activates Rho1 and effector Rho Kinase and these functionally overlap with Death Associated Kinase (Drak) by phosphorylating myosin-2 light chain (Crawford et al. 1998, Royou et al. 2004, Grosshans et al. 2005, Padash Barmchi et al. 2005,

Krajcovic et al. 2012, Chougule et al. 2016, Xue and Sokac 2016, Krueger et al. 2019,). The subsequent activation of myosin-2 motor is requisite for ring assembly. The first proper shape the actomyosin rings take is a hexagonal one (Figure 1 B2', B2''). This 'hexagonal phase' begins at around 4 µm front depth (Figure 1 B2) and ends at around 7 µm front depth (Krueger et al. 2019, This study). The actomyosin rings conformation change into a hexagonal shape is guided by crosslinkers bottleneck and cheerio (Krueger et al. 2019). These same actin regulators also prevent the premature contraction of the rings by stopping myosin-2 contraction through preventing actin filament sliding (Krueger et al. 2019).

Actomyosin rings form into a circular shape roughly between depths of 7 µm and 10 µm (Krueger et al. 2019, This study). The ring phase happens concurrently with the start of the fast-furrowing phase at around 10 µm front depth (Figure 1 B3, B3', B3'') (Krueger et al. 2019, This Study). This rounding is also dependent on myosin-2 motor activity (Xue and Sokac 2016, Krueger et al. 2019). The actin regulators active during the rounding phase include crosslinkers, severing protein Cofilin and filament-bending protein Peanut/Septin 3 as well as the Src kinase (Field and Alberts 1995, Field et al. 2005, Mavrakis et al. 2014, Xue and Sokac 2016, Krueger et al. 2019). To ensure that the fast constriction phase, which starts after 15 µm front depth, does not happen too soon, endocytosis functions by removing excess contractile machinery during slow furrowing phase (Lee and Harris 2013, Liu et al. 2015, Lee et al. 2015, Xue and Sokac 2016,). This fast constriction phase continues all the way up until the end of the invagination at around 30-35 µm front depth (Figure 1 B4) after which the bottoms close (Figard et al. 2013, Kreuger et al. 2016). During the fast constriction phase the actomyosin rings upkeep their circular conformation (Figure 1 B4', B4'') (Xue and Sokac 2016, This Study). Correct architecture and polymerization of the F-actin at the actomyosin rings is vital for a successful fast ring contraction (Mavrakis et al. 2014, Krueger et al. 2016, Xue and Sokac 2016).

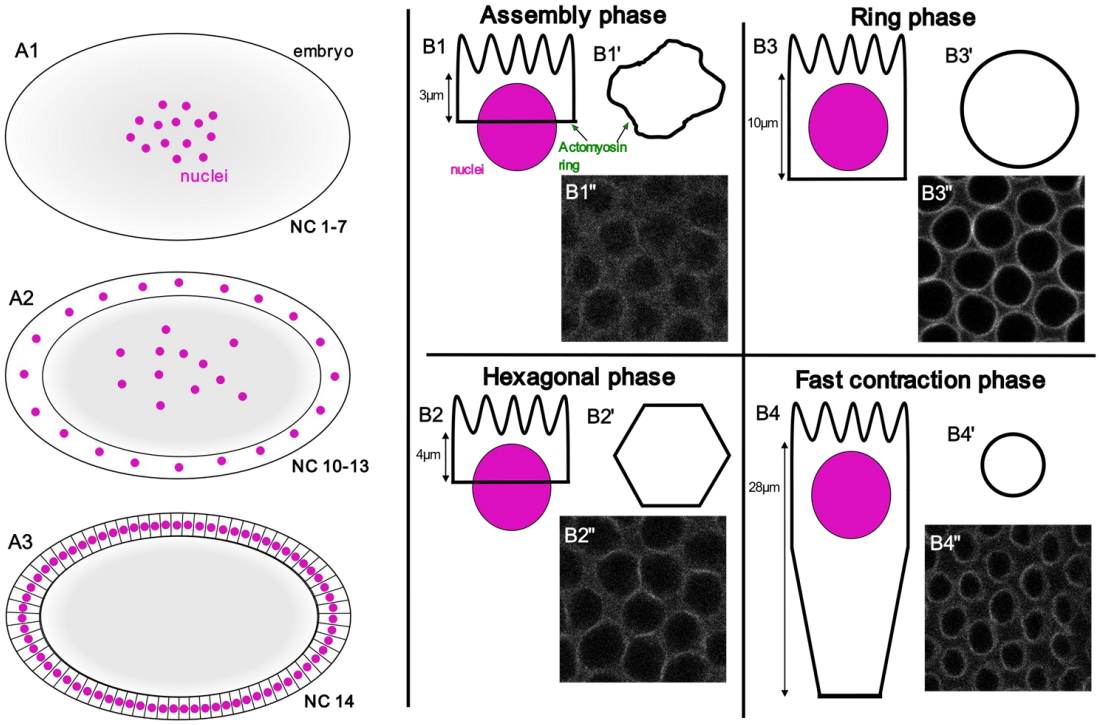

Figure 1: Phases preceding cellularization shown from the embryo level (A1-3) and cellularization phases shown from the cellularization front from top-down view (B1-3) and side view (B1'-B3') as well as confocal microscope image taken from the wild type *Drosophila*'s cellularization front from the indicated depth (B1''-B3''). Nuclei and actomyosin are indicated with purple and green respectively. Nuclei divide close to the center of the embryo through the first nine nuclei cycles (A1). Nuclei start to move to the periphery of the embryo between the 10-13 nuclei cycles (A2). Cellularization happens during the 14th nuclei cycle and results in an epithelial sheet of new cell surrounding the embryo (A3). At the beginning of cellularization at around 3 µm front depth the actomyosin rings form at the cellularization front (B1, B1', B1'') during the assembly phase. The actomyosin rings have obtained a hexagonal shape (B2, B2', B2'') at around 4 µm front depth. Next phase is the circular phase, during which the actomyosin rings achieves a circular shape at around 10 µm front depth (B3, B3', B3''). After the front has passed the nuclei, the actomyosin rings begin their fast contraction phase during which their circular shape remains, but their perimeter reduces rapidly (B4, B4', B4'') This continues until the end of cellularization at around 30-35 µm front depth.

1.5 Study goals and hypotheses

The goal of this study was to expound on the previous knowledge about filamin and the role its MSR has when it comes to filamin interaction with actin, organizing the actin network and binding to plasma membrane. Our study questions were if filamin MSR would affect the structure or the contractile properties of the actin filaments. Another study question was if the filamin MSR would play a part in the binding of actin into the plasma membrane.

To study this we used three different fly genotypes, all of which differed in the required force needed to reveal the cheerio MSR protein interaction sites (Huelssman et al. 2016). Two of these genotypes had a mutation in the MSR (CLOSED and OPEN) while the third was a wild type (WT). CLOSED mutant increased the required force threshold to reveal the protein interaction hidden within, while the OPEN mutant required a very low force to reveal its protein interaction sites.

Our hypothesis relating to the CLOSED genotype was that it would slow down the actomyosin ring dynamics by delaying the formation of the hexagonal ring conformation and having the least amount of variation in its perimeter length. We hypothesize this based on the mutations restricting the OPEN cheerio MSR function as this would reduce and slow its normal function. On the other hand, actomyosin rings on the OPEN genotype would take on the hexagonal conformation earlier than WT and would also show more variation than normal in their perimeter length according to our hypothesis. We believe this would be because the OPEN cheerio MSR is able to interact more efficiently compared to WT and will therefore speed up the normal functioning of cheerio.

Our results showed that decreasing the required force to reveal the MSR interaction sites had the most significant effect on the studied parameters with both perimeter length and circularity as well as the localization of cheerio significantly differing from wild type. These results are consistent with the previous studies suggesting that the filamin C-terminal is responsible for the membrane binding and localization of filamin but goes against suggesting that more interactive prone MSR results in tighter binding to plasma membrane (Huelssman et al. 2016).

2 MATERIALS AND METHODS

2.1 Materials

Genetically modified *Drosophila melanogaster* flies were created by Huelsmann (Huelsmann et al. 2016). Flies were kept at room temperature in plastic 20 ml vials with Nutri-Fly Food (Genesee Scientific, USA).

There were three genotypes used in the experiment (Table 1). All the genotypes had green fluorescent protein (GFP) fused to the C-terminus of cheerio protein. The first genotype is called cher[WT-GFP] (WT) which doesn't have any mutation affecting its function. The two other genotypes were cher[CLOSED MSR] (CLOSED), which had mutations meant to increase the force required to unmask the cheerio MSR's interaction sites, and cher[OPEN MSR] (OPEN), which had mutations meant to decrease the force required to unmask the cheerio MSR's interaction sites.

The fly populations initially included both heterozygotic and homozygotic specimens in terms of the Cheerio MSR mutation. Homozygotic lineages were

successfully created from the WT and CLOSED genotype, but the attempt was unsuccessful for the OPEN genotype (Table 1).

Table 1: Fly genotypes used in the experiment. The first column shows what these genotypes are called in the text. The second column tells the original genotype names. The third column tells the detailed genotype name and shows that the OPEN genotype is heterozygous.

Name used in text	Genotype name	Detailed genotype
WT	cher[WT-GFP]	w;;P{ry[+t7.2]=neoFRT}82B GT{cher[GFP_mGFP6-2]}
CLOSED	cher[CLOSED MSR]	w;;P{ry[+t7.2]=neoFRT}82B GT{cher[closed_mGFP6-2]}
OPEN	cher[OPEN MSR]	w;;P{ry[+t7.2]=neoFRT}82B GT{cher[open_mGFP6-2]}/TM6B,Tb,Hu

2.2 Methods

2.2.1 Preparation for imaging

Before imaging flies were placed into a cage with grape agar bottom (FlyStuff Grape Agar Premix bags, Genesee Scientific) with some yeast added to encourage flies to lay eggs. Eggs were picked 2-3 h after replacing the bottom with a fresh one. To visualize eggs, halocarbon oil 27 (Sigma-aldrich) was added on the plate and eggs were selected under a stereomicroscope. Excess oil was blotted with a piece of tissue paper, and the eggs were submerged in household bleach for a minute to remove the chorion. The eggs were then submerged into three drops of water to wash leftover bleach. Finally, the eggs were then placed onto No. 1.5H 35 mm high glass bottom imaging dish (ibidi) submerged in PBS supplemented with 1 mM ascorbate.

2.2.2 Confocal microscope

The live imaging was performed using Leica SP8 Falcon DMI8-CS confocal microscope (Leica-microsystems) with a tunable Diode white light laser set as 488 nm and 0.7% laser power. The objective used was HC PL APO CS2 63x/1.20 with water immersion. The detector was a hybrid detector (HyD) with 495-740 nm wavelength. The samples were imaged in 3-minute intervals (format: 256x256 pixels, pixel size: 0.08, scan speed: 600 Hz, Zoom: 9, z-stack depth: 40.584 µm, z-step: 0.356 µm). The microscope was operated with Leica Application Suite X (Leica-microsystems).

2.2.3 Image analysis

3D time series data was analyzed with FIJI (v. 1.54f) (Schindelin et al. 2012). At each time point, the depth of cellularization was measured with Plot Z axis Profile tool (Figure 2 A) by plotting the mean fluorescence intensity in each z-slice. The front depth was obtained by measuring the distance from the fluorescence maximum at the surface of embryo and cellularization front.

The actomyosin ring circularity and perimeter was measured at every 3-minute interval timepoint. Multiple slices (3-5) of the image stack, from both side of the of the front, were merged with max intensity Z-projection (Figure 2 B1). This merged image was analyzed using plugin Noise2Void (Krull et al. 2019) (CBSdeep, v.0.6.0) with parameters axes=XY, batchsize=10, numtiles=1, showprogressdialog=true, convertoutputtoinputformat=false. The model for denoising was trained using multiple z-slice (3-5) Z-projections of early and late embryo stage data of randomly selected 3D time series used in the study. The denoised image (Figure 2 B2) was changed to 8-bit and modified: 'auto threshold' (method=Li white), 'despeckle', 'remove outliers' (radius=6 threshold=50 which=Bright), 'remove ourtliers' (radius=6 threshold=50 which=Dark) and the shapes were refined with plugin 'shape smoothing' (v.1.2) (relative_proportion_fds=10, absolute_number_fds=2, keep=[Relative_proportion of FDs] black). The resulting image (Figure 2 B3) was analyzed with 'analyze particles' (size=500-Infinity pixel, circularity=0.8-1.00, show=Outlines display exclude clear) (Figure 2 B4) (Appendix 1).

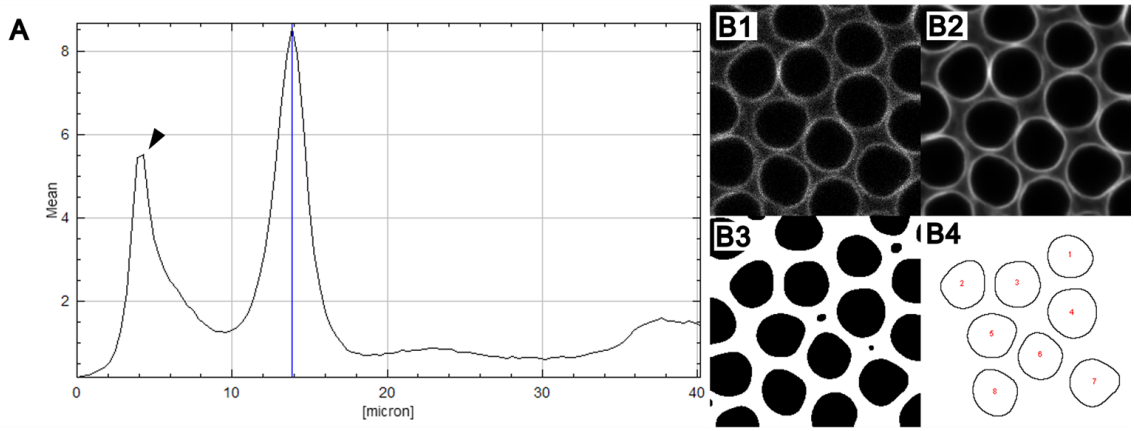

Figure 2: Example of front's depth determination and different steps of analysis of the confocal microscope images, both performed with FIJI. A: FIJI's Plot Z axis Profile tool used to measure the front depth. The mean intensity of the signal is at y-axis and the depth (um) is at the x-axis. The autofluorescent intensity maximum at the embryo surface is indicated with an arrow and the GFP intensity maximum at the cellularization front is indicated with the blue vertical line. The front depth is the distance between these two maxima. B1 is the maximal intensity Z-projection of 5 optical slices around the cellularization front, B2 is the corresponding image after Noise2Void treatment, B3 is the image where the low intensity areas within the high GFP-rings have been segregated and B4 is the resulting image showing the inner edges of the actomyosin rings.

2.2.4 Statistical analysis

For statistical analyses R (v.4.3.1) and RStudio (v.4.3.1) were used. Statistics that were analyzed included filamin ring perimeter length and circularity values. First the outliers from these values were identified (Appendix 1). Outliers were searched separately for each genotype by using the interquartile method. Data point was identified as an outlier if it was more than 1,5 times below the lower fence or 1,5 times above the upper fence. The values in the data that were identified as outliers were removed before moving to other statistical calculations. The Shapiro-Wilk test (Appendix 1) was used to for normality and Levene test (Appendix 1) was used to calculate the homogeneity of variance. The ANOVA test (Appendix 1), with Tukey for multiple comparison, was used to find out significant differences.

3 RESULTS

3.1 Filamin in the cellularization front is less localized around the nuclei in the OPEN genotype compared to other genotypes

To study the effect of filamin mechanosensory region mutations in cellularization, confocal time-laps imaging of embryos carrying GFP-tagged WT cheerio and CLOSED or OPEN mechanosensory region mutants was performed. Most notable differences in filamin localization at the cellularization front were seen between WT and the OPEN mutant. The OPEN mutant showed diffuse localization at the cellularization front between nuclei (Figure 3 C1-C4), whereas WT and CLOSED filamin localized at a concentrated ring near the nuclei (Figure 3 A1-4, B1-4). This difference remained as the cellularization front moved deeper and the filamin rings contracted (Figure 3 A2, B2, C2). The filamin mechanosensory mutations did not have a notable effect on the burrowing rates of the cellularization front (Appendix 3).

The WT and CLOSED side views at 10 µm (Figure 3 A3, B3; Appendix 2) showed the front as a tear shape, with filamin located at the middle and apex of the front with a tail-like runoff towards the surface of the cell. The tear shapes were also clearly separated with large areas of no filamin between them. The OPEN side view (Figure 3 C3, Appendix 2) was otherwise similar to the two other genotypes, but with a weaker signal. At 20 µm depth the filamin was less visible within all genotypes likely because the signal was weaker at lower depths but might also indicate that there was less filamin present at the front. As the filamin rings constricted during front progression the previously individual tears seemed to have merged somewhat and were no longer clearly separated (Figure 3, Appendix 2).

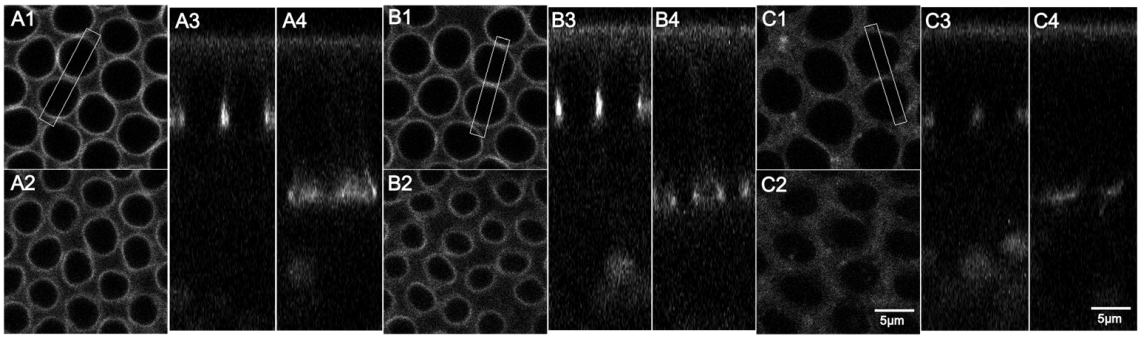

Figure 3: Filamin localization during cellularization. Filamin localization follows similar patterns between WT and CLOSED genotypes but is more diffused in the OPEN genotype. Filamin localization in the cellularization front visualized with A) WT, B) CLOSED and C) OPEN fly genotypes. Figure shows the top-down view of the cellularization front from the depths of 10 µm (A1, B1 and C1) and 20 µm (A2, B2 and C2) as well as the side view of the cellularization front from the depths of 10 µm (A3, B3 and C3) and 20 µm (A4, B4 and C4). A1, A2, B1, B2, C1 and C2 are z-projections created from five z-stack slices. The boxes in A1, B1 and C1 depict the volume where the A3-A4, B3-B4, and C3-C4 projections are shown.

3.2 The filamin rings of the OPEN genotype separated themselves with their perimeter length and circularity compared to other two genotypes

To quantitatively analyze the differences in the filamin ring size and shape during cellularization, likely affected by myosin contraction activity and organization of the actin fibers respectively, the nuclear rings were segregated from the images and their perimeter length and circularity analyzed. During the early phase of cellularization the rings grow to their maximum perimeter length and go through a small contraction, which ends when the front depth is around 10 µm. At this phase, the OPEN genotype reached longer perimeter length than the two other genotypes (Figure 4 A1). ANOVA analysis with Tukey post hoc test taken from maximum perimeter of three value averages before 10 µm depth (3,2–9,6 µm) showed significant difference ($p<0.032$) between WT and OPEN samples while comparison between CLOSED and OPEN was close to significant ($p<0.063$) (Figure 4 B1). The mean maximum perimeter length was 18.2 ± 0.7 µm in WT (n=10), 18.5 ± 0.4 µm in CLOSED (n=10) and 20.6 ± 0.7 µm in OPEN (n=7).

After passing 10 µm depth, the rings go through a second larger contraction, which finally leads to the closure of membrane under the nuclei. During this late phase of cellularization, the perimeter length of OPEN filamin remained notably larger compared to the two other types (Figure 4 A1). Three value average perimeter length measurements starting from front depth closest to 15 µm were compared between all genotypes (Figure 4 B2). The mean perimeter length was 14.4 ± 0.6 µm in WT (n=10), 13.2 ± 0.4 µm in CLOSED (n=10) and 18.2 ± 0.6 µm in OPEN (n=5). The ANOVA with Tukey post hoc test showed significant difference both between WT and OPEN ($p<0.0007$) as well as CLOSED and OPEN ($p<0.00003$).

Average circularity of the rings initially followed similar trend in all the genotypes as the front depth increased, but later from 10 µm front depth onward the OPEN diverged from the other two types (Figure 4 A2). The maximum circularity values were achieved at around 10 µm front depth. The circularity of the OPEN type followed a very different route compared to other types as it begins to decrease earlier after obtaining its largest circularity values. The decrease began at around 10 µm and continued almost all the way till the end of measurements. The variation of the individual circularity values was largest from 10 µm depth onward and especially OPEN values had a lot of variation during the decrease of its circularity. This can be seen well with the increase of the variation of the standard error around the average circularity of OPEN fly type at 25 µm depth onward. To evaluate the difference between genotypes, three value average of circularity measurement, starting from front depth closest to 15 µm, were compared between all genotypes (Figure 4 B3). Perfect circle would have a value of 1. WT circularity was 0.892 ± 0.0029 (n=10), CLOSED circularity was 0.896 ± 0.0041 (n=10) and OPEN circularity was 0.875 ± 0.0054 (n=6). ANOVA test with Tukey post hoc test for multiple comparisons gave both WT–OPEN ($p<0.022$) and CLOSED–OPEN ($p<0.0062$) comparisons significant differences.

Overall, OPEN type was clearly different from the two other genotypes in terms of perimeter and circularity changes per depth. It upheld a larger average perimeter almost throughout the cellularization while its circularity stayed lower than the two other genotypes and decreased strongly throughout the contraction of its perimeter. Individual data values, especially in the case of circularity, showed less variation at the beginning. This variation, however, increased as the fronts moved deeper and is particularly noticeable with the OPEN genotype.

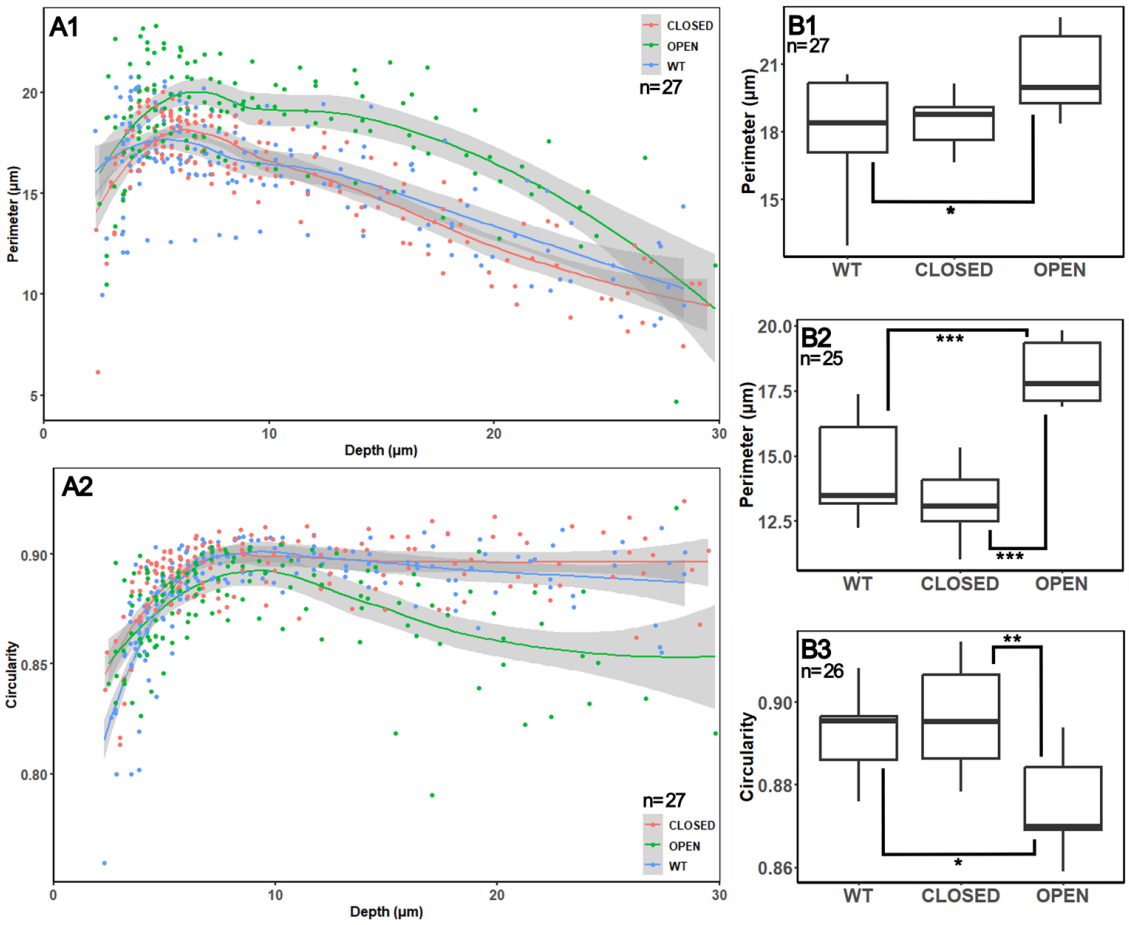

Figure 4: Perimeter length and circularity of filamin rings at the cellularization front. In both aspects OPEN genotype deviated from WT and CLOSED. In A1 the colored solid lines show the average perimeter length (µm) as a function of depth (µm) and the colored dots show all measurements from the corresponding genotype. In A2 the average circularity and all measurements are similarly shown. Standard error is represented as the gray area around the average line. In both A1 and A2 the red color represents CLOSED genotype (n=10), green OPEN genotype (n=7) and blue WT genotype (n=10). Actomyosin rings' perimeter length and circularity statistical analyses were taken from two different areas of depth. In all these cases a three data value average was taken from each sample. Maximum perimeter length measurements from below 10 µm front depth (B1) included measurements taken from depths between 3,2–9,6 µm while the average depth was 5,4 µm. Perimeter length (B2) and circularity (B3) measurements were taken with the first data value closest to 15 µm depth (13-16 µm) and the last data value between 17-25 µm. The average distance of depth covered per sample in B2 and B3 was 6,1 µm but reached from 3 to 12 µm. In B1-B3 the vertical line below and above the box shows the 25 % of the lowest and highest sample values respectively. The horizontal line across the box shows the mean value of the samples and the area of the box below and above the mean line shows the 25 % of the sample values below and above the mean value respectively. The stars between the sample pairs in B1-3 indicates significant difference with * = $p < 0,05$; ** = $p < 0,01$ and *** = $p < 0,001$.

4 DISCUSSION

This study aimed to elucidate the role of the cheerio's MSR during *Drosophila's* cellularization. We were also interested to see what effects the disruption of the normal cheerio MSR masking site might have. The tested cheerio crosslinkers varied in the required force to reveal their protein interaction site masked by the MSR. The effects of the OPEN mutant cheerio were surprisingly strong. These effects were seen in the actomyosin ring perimeter length and circularity as well as in the localization of actomyosin on the cellularization front. When it comes to hypothesis relating to OPEN genotype, it did have the largest change in respect to perimeter length per depth at least during early cellularization, but didn't obtain hexagonal shape faster than WT. On the other hand, the CLOSED genotype results went against the hypothesis as they were practically identical with the WT.

4.1 OPEN cheerio mutant affected the distribution and the dynamics of the actomyosin ring

The OPEN mutant cheerio seems to affect the perimeter length and circularity of the actomyosin rings by increasing the former and lowering the latter. The lower circularity can be seen to a lesser degree during early cellularization, but it is especially distinct during late cellularization. The higher perimeter can be seen throughout the cellularization. These effects during late cellularization are quite fascinating as cheerio is normally responsible for the formation and upkeep of the hexagonal shape during early cellularization (Krueger et al. 2019). In addition, the MSR bearing C-terminal has previously not been associated with affecting the actin structure (Huelsmann et al. 2016). These results however point towards MSR region having the potential to affect the actomyosin organization. One can assume that normally during the hexagonal phase actomyosin rings have lower circularity and comparable or higher perimeter length compared to circular conformation. These traits, especially the higher perimeter, are amplified in the OPEN mutant. OPEN cheerio's potential for increased activity might enable the actomyosin ring to express more distinct hexagonal traits. This could happen through the OPEN mutation stabilizing actin structure and hence the actin itself leading to reduced dynamics of the actomyosin ring. Interestingly, while the OPEN perimeter is larger compared to WT it still follows some similar patterns. For example, the slow constriction happens at similar depths within all the genotypes and ends at around 10 µm depth. This seems to suggest that the OPEN cheerio mutant does not alter the timing of this first slow constriction. This is possibly because the first constriction is facilitated by myosin-2 motor activity

rather than F-actin of which assembly is controlled by cheerio among other actin regulators (Xue and Sokac 2016).

Cheerio appears at the basal level at start of the cellularization and increases in concentration until reaching a plateau at the end of the hexagonal phase and remaining at the basal level throughout cellularization (Krueger et al. 2019). The structural organization of actin determines its contractile properties and the hexagonal shape is resistant to myosin-II activity required in the transition to ring conformation (Reymann et al. 2012, Ennomani et al. 2016, Xue and Sokac 2016). In addition, F-actin disassembly plays a large part in the constriction during phase 2 or fast constriction (Xue and Sokac 2016). Based on this perhaps the OPEN cheerio's increased activity works to stabilize and prolong the hexagonal shape and resists the disassembly which in turn delays the beginning of fast constriction.

Interestingly OPEN cheerio seems to localize differently compared to other genotypes. It is dispersed equally around the space between the openings, instead of concentrating around the edges of the membrane openings like other genotypes. The human filamin is known to be able to interact with various proteins with the interaction site for most of these at or around the MSR (Feng and Walsh, 2004). This presents a question if the more interactive OPEN cheerio MSR can interact with other components on the route to or at the cellularization front and if these potential new interactions could affect cheerio's localization and function. This hypothesis is supported by the previously mentioned filamin C-terminal's is more active role in binding to membrane compared to N-terminal (Huelsmann et al. 2016). This way modified MSR could explain the cheerio's abnormal localization. Previously OPEN cheerio has been shown to be more tightly connected to the plasma membrane (Huelsmann et al. 2016). This makes it surprizing that OPEN cheerio is shown to delocalize this much. It is unlikely that the mutations would affect cheerio’s ability to bind onto actin as its actin binding site is opposite end of the site of MSR and unaffected by the mutations (Huelsmann et al. 2016). Based on this we could assume that the site of the imaged cheerio is also the site of actin and that in OPEN fronts the actin is similarly disorganized. On the other hand, there are numerous other actin binding components like bottleneck and fimbrin during different phases of the cellularization (Krueger et al. 2019). The OPEN cheerio might be unable to disorganize actin to this effect if other actin binding components are functioning normally and likely attempting to localize actin correctly. Alternatively, it might be possible that OPEN cheerio can get misdirected during its route to the basal area and localize away from the front. This however is not collaborated by the side view (Appendix 2) as this does not indicate that OPEN cheerio is localized differently in terms of depth compared to CLOSED and WT.

4.2 CLOSED cheerio mutant did not have effect on either the distribution or the dynamics of the actomyosin ring

CLOSED cheerio did not affect the circularity or the perimeter length of the actomyosin rings during cellularization. Both of these perimeters followed the WT trends quite closely. The seemingly similar functions between CLOSED and WT could be because the higher force threshold for MSR interaction in the CLOSED cheerio, caused by their mutation, isn't enough to disrupts the cheerio's normal function. Studies done with cheerio knockdown shows that it prevented the formation of hexagonal rings and lead to premature rounding and constriction (Krueger et al. 2019). CLOSED cheerio does not show similar effect on the cellularization front. This suggests that CLOSED mutant does not inactivate or deter the normal functionality of cheerio during cellularization, at least to any significant effect.

The CLOSED mutant does not appear to affect the localization of cheerio. The front images show cheerio localization in the CLOSED genotype to be identical to the WT genotype. This could be because CLOSED mutation was not enough to deter the normal localization of cheerio or because the localization is controlled by factors other than cheerio. The OPEN cheerio's differing localization suggests that the former is correct. Even if this is the case it is still unclear whether the cheerio's localization is solely dependent on the MSR activity, or whether the MSR activity is just one of multiple factors controlling it.

4.3 Limitations and future prospects

There are some limitations relating to this study that are good to keep in mind. First relates to the OPEN genotype being the only one that is heterozygotic in terms of its cheerio MSR mutation. This fact makes it unclear if the OPEN phenotype would be intensified or altered by its homozygotic version or if it can be directly compared to the homozygotic versions of the other genotypes. OPEN's heterozygotic nature also makes the perimeter length and especially circularity results at higher depths more unreliable because of the lower signal intensity. This is further shown by the high variation of the perimeter length and circularity in the OPEN genotype at higher depths. Circularity results at higher depths in the OPEN genotype are especially unreliable as the dispersed localization of the cheerio and the low signal makes the precise defining of the borders around the opening difficult. In addition, it is unclear if the measured OPEN circularity values are completely trustworthy as they could refer more to the borders around the opening without actin rather than to the actin rings themselves. The image analysis methods used to achieve the perimeter length and circularity were new and would therefore require more refining to be made more precise and reliable. In addition, because the measurements from the front were done with a FIJI macro it was important to ensure the reliability of the results by manually looking them through. One potential improvement would be to analyze the openings at the front separately, but this would notably increase

the required workload. Alternatively, the opening could be analyzed manually, but again the workload would increase considerably. The ideal workload would likely consist of automatic analysis of most of the images with manual analysis of some lower quality images and a thorough manual overview of the results to catch any mistakes made by either automatic or manual analyses. Lastly for future studies it would also be ideal to imagine a larger number of flies from each genotype as the number of flies imaged for this study, especially the OPEN flies, was quite low.

The overall results indicate that modification of the MSR site can affect the cellularization phenotype but does not answer the exact role of MSR region during cellularization. In addition, we do not know what proteins interact with cheerio MSR or if these only interact with OPEN cheerio MSR. Whether these components are present throughout the cellularization process or only during certain phases is also an interesting question. Revealing the interplay between MSR and these components would likely elucidate the reasons for the differences seen between OPEN and WT genotypes. The results also raise the question if the OPEN cheerio that is shown to be localized away from the actomyosin rings' usual location also causes the actin to delocalize by binding to it or if other actin crosslinkers or other mechanisms can deter this. Similarly, the delocalization of OPEN cheerio brings into question if it truly affects the organization of the actomyosin structure because of its and actin's potential delocalization. Therefore, it would be interesting to see how the actin is localized in the OPEN genotype. When it comes to CLOSED genotype, it would be interesting to study if even higher force requirement would deter the functionality of cheerio and if this would result in a similar phenotype as seen with cheerio knockdown in 2019 study from Krueger. Of course, being able to get results from homozygotic OPEN genotype, would also be interesting as it would show if the results seen in this study would be amplified or if they would differ.

5 CONCLUSIONS

This study produced results suggesting that the cheerio MSR region plays a role in the circularity and perimeter length of the actomyosin rings during *Drosophila* cellularization. It also appears to affect the cheerio's localization at the front. These differences were only observed in OPEN genotype, likely caused by its cheerio's revealed MSR having abnormal activity. Because OPEN cheerio showed significantly different results compared to WT and CLOSED, it could be that there are forces affecting the OPEN cheerio MSR that do not normally reach the force threshold required to interact with WT cheerio MSR. The OPEN genotype seems to affect the cellularization by increasing the normal function of cheerio. It also seems to affect the localization of cheerio by disorganizing it across the cellularization front. It is not clear whether these traits are due to distortion of the normal MSR functions, the MSR interacting with components it wouldn't interact with during normal cellularization or a mixture of both. Based on the similar phenotype between WT and CLOSED genotypes, the forces acting on the MSR region during cellularization are strong enough to ensure the normal function of CLOSED cheerio MSR despite the higher force requirement to reveal its MSR interaction sites.

ACKNOWLEDGEMENTS

Supervisors Professor Jari Ylänne and MSc Riku Korkiamäki
Funding from Research Council of Finland

Jyväskylä May 8, 2024
Mikko Hakanen

REFERENCES

Acharya S., Laupsien P., Wenzl C., Yan S. & Grosshans J. 2014. Function and dynamics of slam in furrow formation in early Drosophila embryo, *Dev. Biol.* 386 (2) 371–384. doi:10.1016/j.ydbio.2013.12.022.

Agarwal, P. & Zaidel-Bar R. 2019. Principles of Actomyosin Regulation In Vivo. *Trends Cell Biol.* 29:150–163. doi:10.1016/j.tcb.2018.09.006.

Belmonte J.M., Leptin M., & Nédélec F. 2017. A theory that predicts behaviors of disordered cytoskeletal networks. *Mol. Syst. Biol.* 13:941. doi:10.15252/msb.20177796.

Bendix P.M., Koenderink G.H., Cuvelier D., Dogic Z., Koeleman B.N., Brieher W.M., Field C.M., Mahadevan L. & Weitz D.A. 2008. A quantitative analysis of contractility in active cytoskeletal protein networks. *Biophys. J.* 94:3126–3136. doi:10.1529/biophysj.107.117960.

Blanchoin L., Boujemaa-Paterski R., Sykes C., & Plastino J. 2014. Actin dynamics, architecture, and mechanics in cell motility. *Physiol. Rev.* 94: 235–263. doi:10.1152/physrev.00018.2013.

Cao J., Albertson R., Riggs B., Field C.M. & Sullivan W. 2008. Nuf, a Rab11 effector, maintains cytokinetic furrow integrity by promoting local actin polymerization. *J. Cell Biol.* 182 (2) 301–313. doi:10.1083/jcb.200712036.

Chougule A.B., Hastert M.C. & Thomas J.H. 2016. Drak is required for actomyosin organization during drosophila cellularization. *G3* 6 (4) 819–828. doi:10.1534/g3.115.026401.

Chugh P., Clark A.G., Smith M.B., Cassani D.A.D, Dierkes K., Ragab A., Roux P.P., Charras G., Salbreux G. & Paluch E.K. 2017. Actin cortex architecture regulates cell surface tension. *Nat. Cell Biol.* 19:689–697. doi:10.1038/ncb3525.

Chugh P. & Paluch E.K. 2018. The actin cortex at a glance. *J. Cell Sci.* 131 (14). doi:10.1242/jcs.186254.

Crawford J.M., Harden N., Leung T., Lim L. & Kiehart D.P. 1998. Cellularization in Drosophila melanogaster is disrupted by the inhibition of rho activity and the activation of Cdc42 function. *Dev. Biol.* 204 (1) 151–164. doi:10.1006/dbio.1998.9061.

Ennomani H., Letort G., Guérin C., Martiel J.L., Cao W., Nédélec F., De La Cruz E.M., Théry M. & Blanchoin L. 2016. Architecture and Connectivity Govern Actin Network Contractility. *Curr. Biol.* 26:616–626. doi:10.1016/j.cub.2015.12.069.

Feng Y., Walsh C. 2004. The many faces of filamin: A versatile molecular scaffold for cell motility and signalling. *Nat Cell Biol* 6, 1034–1038. doi:10.1038/ncb1104-1034.

Field C.M. & Alberts B.M. 1995. Anillin, a contractile ring protein that cycles from the nucleus to the cell cortex. *J. Cell Biol.* 131 (1) 165–178. doi:10.1083/jcb.131.1.165.

Field C.M., Coughlin M., Doberstein S., Marty T. & Sullivan W. 2005. Characterization of anillin mutants reveals essential roles in septin localization and plasma membrane integrity. *Development* 132 (12) 2849–2860. doi:10.1242/dev.01843.

Figard L., Xu H., Garcia H.G., Golding I. & Sokac A.M. 2013. The plasma membrane flattens out to fuel cell-surface growth during Drosophila cellularization. *Dev. Cell* 27 (6) 648–655. doi:10.1016/j.devcel.2013.11.006.

Figard L., Wang M., Zheng L., Golding I. & Sokac A.M. 2016. Membrane supply and demand regulates F-Actin in a cell surface reservoir. *Dev. Cell* 37 (3) 267–278. doi:10.1016/j.devcel.2016.04.010.

Foe V.E. & Alberts B.M. 1983. Studies of nuclear and cytoplasmic behaviour during the five mitotic cycles that precede gastrulation in Drosophila embryogenesis. *J. Cell Sci.* 61 31–70. doi:10.1242/jcs.61.1.31.

Gorlin J.B., Yamin R., Egan S., Stewart M., Stossel T.P., Kwiatkowski D.J. & Hartwig J.H. 1990. Human endothelial actin-binding protein (ABP-280, nonmuscle filamin): a molecular leaf spring. *J. Cell Biol.* 111, 1089–1105. doi: 10.1083/jcb.111.3.1089.

Grosshans J., Wenzl C., Herz H.M., Bartoszewski S., Schnorrer F., Vogt N., Schwarz H. & Muller H.A. 2005. RhoGEF2 and the formin Dia control the formation of the furrow canal by directed actin assembly during Drosophila cellularisation. *Development* 132 (5) 1009–1020. doi:10.1242/dev.01669.

Hartwig J.H. & Stossel T.P. 1975. Isolation and properties of actin, myosin, and a new actinbinding protein in rabbit alveolar macrophages. *The Journal of biological chemistry*, *250*(14), 5696–5705.

Hartwig H.H. & Stossel T.P. 1981. Structure of macrophage actin-binding protein molecules in solution and interacting with actin filaments. *J Mol Biol*, 145:563-581. doi:10.1016/0022-2836(81)90545-3.

He B. & Martin A. 2016. Wieschaus E., Flow-dependent myosin recruitment during Drosophila cellularization requires zygotic dunk activity. *Development* 143 (13) 2417–2430. doi:10.1242/dev.131334.

Holly R.M., Mavor L.M., Zuo Z. & Blankenship J.T. 2015. A rapid, membrane-dependent pathway directs furrow formation through RalA in the early Drosophila embryo. *Development* 142 (13) 2316–2328. doi:10.1242/dev.120998.

Huelsmann S., Rintanen N., Sethi R., Brown N.H. & Ylänne J. 2016. Evidence for the mechanosensor function of filamin in tissue development. *Sci Rep*. Sep 6;6:32798. doi: 10.1038/srep32798.

Kelkar M., Bohec P. & Charras G. 2020. Mechanics of the cellular actin cortex: From signalling to shape change. *Curr. Opin. Cell Biol.* 66 69–78. doi:10.1016/j.ceb.2020.05.008.

Koenderink G.H. & E.K. Paluch. 2018. Architecture shapes contractility in actomyosin networks. *Curr. Opin. Cell Biol.* 50:79–85. doi:10.1016/j.ceb.2018.01.015.

Krajcovic M.M. & Minden J.S. 2012. Assessing the critical period for Rho kinase activity during Drosophila ventral furrow formation. *Dev. Dyn.* 241 (11) 1729–1743. doi:10.1002/dvdy.23859.

Kramerov A.A., Mikhaleva E.A., Rozovsky Ya.M., Pochechueva T.V., Baikova N.A., Arsenjeva E.L. & Gvozdev V.A. 1997. Insect mucin-type glycoprotein: immunodetection of the O-glycosylated epitope in Drosophila melanogaster cells and tissues. *Insect Biochem Mol Biol*, 27:513-521. doi:10.1016/s0965-1748(97)00026-x.

Krueger D., Quinkler T., Mortensen S.A., Sachse C., De Renzis S. 2019. Cross-linker-mediated regulation of actin network organization controls tissue morphogenesis. *J Cell Biol.* Aug 5;218(8):2743-2761. doi:10.1083/jcb.201811127.

Krull A., Buchholz T. O. & Jug F. 2019. Noise2void-learning denoising from single noisy images. *Proceedings of the IEEE/CVF conference on computer vision and pattern recognition* (pp. 2129-2137).

Laporte D., Ojkic N., Vavylonis D. & Wu J.Q. 2012. α-Actinin and fimbrin cooperate with myosin II to organize actomyosin bundles during contractile-ring assembly. *Mol. Biol. Cell.* 23:3094–3110. doi:10.1091/mbc.E12-02-0123.

Lecuit, T. & Wieschaus E. 2000. Polarized insertion of new membrane from a cytoplasmic reservoir during cleavage of the Drosophila embryo. *J. Cell Biol.* 150:849–860. doi:10.1083/jcb.150.4.849.

Lecuit T. 2004. Junctions and vesicular trafficking during Drosophila cellularization. *J. Cell Sci.* 117 (16) 3427–3433. doi:10.1242/jcs.01312.

Lee D.M. & Harris T.J. 2013. An Arf-GEF regulates antagonism between endocytosis and the cytoskeleton for Drosophila blastoderm development. *Curr. Biol.* 23 (21) 2110–2120. doi:10.1016/j.cub.2013.08.058.

Lee D.M., Rodrigues F.F., Yu C.G., Swan M. & Harris T.J. 2015. PH Domain-Arf, G protein interactions localize the Arf-GEF steppke for cleavage furrow regulation in drosophila. *PLoS One* 10 (11), e0142562. doi:10.1371/journal.pone.0142562.

Levayer, R. & Lecuit T. 2012. Biomechanical regulation of contractility: spatial control and dynamics. *Trends Cell Biol.* 22:61–81. doi: 10.1016/j.tcb.2011.10.001.

Li M.G., Serr M., Edwards K., Ludmann S., Yamamoto D., Tilney L.G., Field C.M. & Hays T.S. 1999. Filamin is required for ring canal assembly and actin organization during Drosophila oogenesis. *J. Cell Biol.* 146: 1061–1074. doi:10.1083/jcb.146.5.1061.

Liu J., Lee D.M., Yu C.G., Angers S. & Harris T.J. 2015. Stepping stone: a cytohesin adaptor for membrane cytoskeleton restraint in the syncytial Drosophila embryo. *Mol. Biol. Cell* 26 (4) 711–725. doi:10.1091/mbc.E14-11-1554.

Mavor L.M., Miao H., Zuo Z., Holly R.M., Xie Y., Loerke D. & Blankenship J.T. 2016. Rab8 directs furrow ingression and membrane addition during epithelial formation in Drosophila melanogaster. *Development* 143 (5) 892–903. doi: 10.1242/dev.128876.

Mavrakis M., Azou-Gros Y., Tsai F.C., Alvarado J., Bertin A., Iv F., Kress A., Brasselet S., Koenderink G.H. & Lecuit T. 2014. Septins promote F-actin ring formation by crosslinking actin filaments into curved bundles. *Nat. Cell Biol.* 16 (4) 322–334. doi:10.1038/ncb2921.

Murrell, M., Oakes P.W., Lenz M., & Gardel M.L. 2015. Forcing cells into shape: the mechanics of actomyosin contractility. *Nat. Rev. Mol. Cell Biol.* 16:486–498. doi:10.1038/nrm4012.

Murthy M., Teodoro R.O., Miller T.P. & Schwarz T.L. 2010. Sec5, a member of the exocyst complex, mediates Drosophila embryo cellularization. *Development* 137 (16) 2773–2783. doi:10.1242/dev.048330.

Ohta Y. & Hartwig J.H. 1996. Phosphorylation of actin-binding protein 280 by growth factors is mediated by p90 ribosomal protein S6 kinase. *J Biol Chem* 1996, 271:11858-11864. doi:10.1074/jbc.271.20.11858.

Padash Barmchi M., Rogers S. & Hacker U. 2005. DRhoGEF2 regulates actin organization and contractility in the Drosophila blastoderm embryo. *J. Cell Biol.* 168 (4) 575–585. doi:10.1083/jcb.200407124.

Pollard T.D. & Wu J.Q. 2010. Understanding cytokinesis: lessons from fission yeast. *Nat. Rev. Mol. Cell Biol.* 11:149–155. doi:10.1038/nrm2834.

Reymann A.C., Boujemaa-Paterski R., Martiel J.L., Guérin C., Cao W., Chin H.F., De La Cruz E.M., Théry M. & Blanchoin L. 2012. Actin network architecture can determine myosin motor activity. *Science.* 336: 1310–1314. doi:10.1126/science.1221708.

Rognoni L., Stigler J., Pelz B., Ylänne J. & Rief M. 2012. Dynamic force sensing of filamin revealed in single-molecule experiments. *Proc. Natl. Acad. Sci.* 109, 19679–19684. doi:10.1073/pnas.1211274109.

Royou A., Field C., Sisson J.C., Sullivan W. & Karess R. 2004. Reassessing the role and dynamics of nonmuscle myosin II during furrow formation in early Drosophila embryos. *Mol. Biol. Cell* 15 (2) 838–850. doi:10.1091/mbc.e03-06-0440.

Schejter, E.D., & Wieschaus E. 1993. bottleneck acts as a regulator of the microfilament network governing cellularization of the Drosophila embryo. *Cell.* 75:373–385. doi:10.1016/0092-8674(93)80078-s.

Schindelin J., Arganda-Carreras I. & Frise E. et al. 2012. Fiji: an open-source platform for biological-image analysis. *Nature Methods, 9(7),* 676–682. doi:10.1038/nmeth.2019.

Schmidt A. & Grosshans J. 2018. Dynamics of cortical domains in early Drosophila development. *J. Cell Sci.* 131 (7). doi:10.1242/jcs.212795.

Schmoller K.M., Lieleg O. & Bausch A.R. 2009. Structural and viscoelastic properties of actin/filamin networks: cross-linked versus bundled networks. *Biophys. J.* 97:83–89. doi:10.1016/j.bpj.2009.04.040.

Sokac A.M. & Wieschaus E. 2008. Local actin-dependent endocytosis is zygotically controlled to initiate Drosophila cellularization. *Dev. Cell* 14 (5) 775–786. doi:10.1016/j.devcel.2008.02.014.

Sokac A.M., Biel N. & De Renzis S. 2023. Membrane-actin interactions in morphogenesis: Lessons learned from Drosophila cellularization. *Seminars*

in cell & developmental biology, *133*, 107–122. doi:10.1016/j.semcdb.2022.03.028.

Sokol N.S. & Cooley L. 1999. Drosophila filamin encoded by the cheerio locus is a component of ovarian ring canals. *Curr. Biol.* 9:1221–1230. doi:10.1016/s0960-9822(99)80502-8.

Stendahl O.I., Hartwig J.H., Brotschi E.A. & Stossel T.P. 1980. Distribution of actinbinding protein and myosin in macrophages during spreading and phagocytosis. *J. Cell Biol.* 84, 215–224. doi: 10.1083/jcb.84.2.215.

Stossel T.P., Condeelis J., Cooley L., Hartwig J.H., Noegel A., Schleicher M. & Shapiro S.S. 2001. Filamins as integrators of cell mechanics and signalling. *Nature reviews. Molecular cell biology*, *2*(2), 138–145. doi: 10.1038/35052082.

Su J., Chow B., Boulianne G.L. & Wilde A. 2013. The BAR domain of amphiphysin is required for cleavage furrow tip-tubule formation during cellularization in Drosophila embryos. *Mol. Biol. Cell* 24 (9) 1444–1453. doi:10.1091/mbc.E12-12-0878.

Svitkina T.M. & Borisy G.G. 1999. Arp2/3 complex and actin depolymerizing factor/cofilin in dendritic organization and treadmilling of actin filament array in lamellipodia. *J. Cell Biol.* 145:1009–1026. doi:10.1083/jcb.145.5.1009.

Wang K., Ash J. F. & Singer S. J. 1975. Filamin, a new high-molecular-weight protein found in smooth muscle and non-muscle cells. *Proc. Natl Acad. Sci.* USA 72, 4483–4486. doi:10.1073/pnas.72.11.4483.

Weihing R.R. 1985. The filamins: properties and functions. *Can. J. Biochem. Cell Biol.* 63, 397–413. doi:10.1139/o85-059.

Xue Z., Sokac A.M. 2016. Back-to-back mechanisms drive actomyosin ring closure during Drosophila embryo cleavage. *J. Cell Biol.* November 7; 215 (3): 335–344. doi: 10.1083/jcb.201608025.

Yan S., Lv Z., Winterhoff M., Wenzl C., Zobel T., Faix J., Bogdan S. & Grosshans J. 2013. The F-BAR protein Cip4/Toca-1 antagonizes the formin Diaphanous in membrane stabilization and compartmentalization. *J. Cell Sci.* 126 (8) 1796–1805. doi:10.1242/jcs.118422.

Zhou X., Borén J. & Akyürek L.M. 2007. Filamins in cardiovascular development. Trends Cardiovasc. Med. 17, 222–229. doi: 10.1016/j.tcm.2007.08.001.

Zhou A.X., Hartwig J.H. & Akyürek L.M. 2010. Filamins in cell signaling, transcription and organ development. *Trends Cell Biol*. 2010;20(2):113-123. doi:10.1016/j.tcb.2009.12.001.

APPENDIX 1. MACROS & SCRIPTS

Image analysis macro:

```
Stack.getPosition(channel, slice, frame)
sliceMin=slice-5
sliceMax=slice+5
timeframe1=frame
run("Make Substack...", "channels=1-2 slices=" + sliceMin + "-" + sliceMax +
" frames=" + frame );
rename("SUM2");
//run("Z Project...", "projection=[Max Intensity]");
run("Z Project...", "projection=[Sum Slices]");
rename("SUM");
run("N2V predict", "modelfile=[modelfile.zip] input=SUM axes=XY
batchsize=10 numtiles=1 showprogressdialog=true
convertoutputtoinputformat=false");
selectWindow("output");
run("Duplicate...", " ");
run("8-bit");
run("Auto Threshold", "method=Li white");
run("Despeckle");
run("Remove Outliers...", "radius=6 threshold=50 which=Bright");
run("Remove Outliers...", "radius=6 threshold=50 which=Dark");
run("Shape Smoothing", "relative_proportion_fds=10
absolute_number_fds=2 keep=[Relative_proportion of FDs] black");
run("Analyze Particles...", "size=500-Infinity pixel circularity=0.8-1.00
show=Outlines display exclude clear");
```

Outlier script:

```
library(tidyverse)
library(dplyr)
DATA %>%
group_by(TYPE) %>%
mutate(IQR = IQR(get(values), na.rm = TRUE),
Q1 = quantile(get(values), 0.25, na.rm = TRUE),
 Q3 = quantile(get(values), 0.75, na.rm = TRUE)) %>%
filter((get(values)< (Q1 - 1.5 * IQR)) | (get(values)> (Q3 + 1.5 * IQR)))
```

Shapiro-Wilk script:

```
library(stats)
shapiro.test(Data)
```

Levene script:

```
library(car)
leveneTest(Data)
```

ANOVA script:

```
library(tidyverse)
library(stats)
Data %>%
aov(Data_value ~ Fly_Type, data = .) %>%
TukeyHSD()
```

APPENDIX 2. COLLECTION OF TOPDOWN AND SIDE IMAGES OF THE THREE GENOTYPES

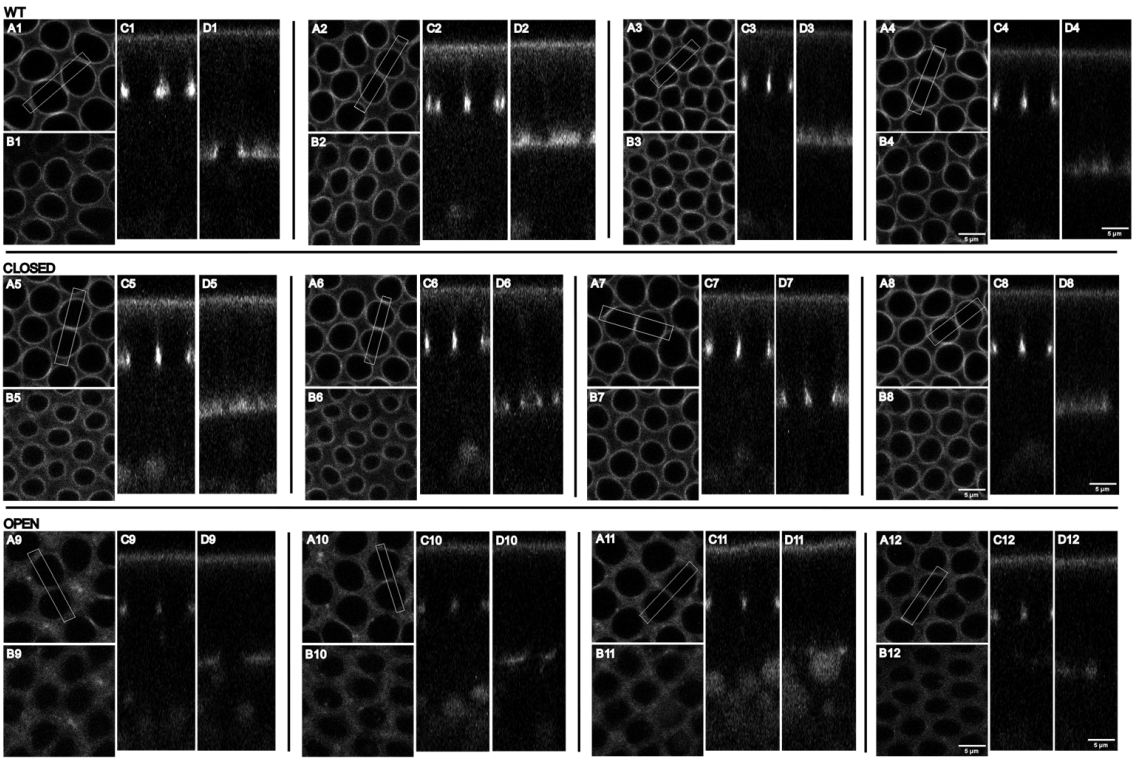

Figure 1: Collection of four samples from all three genotypes. Top row shows WT (A1-4, B1-4, C1-4, D1-4), middle row CLOSED (A5-8, B5-8, C5-8, D5-8) and bottom row OPEN (A9-12, B9-12, C9-12, D9-12) genotype samples. Figure shows the top-down view of the cellularization front from the depths of 10 µm (A1-12) and 20 µm (B1-12) as well as the side view of the cellularization front from the depths of 10 µm (C1-12) and 20 µm (D1-12). Top-down images (A1-12, B1-12) are z-projections created from five z-stack slices. The boxes in A1-12 depict the volume where the side view projections are shown. Horizontal lines separate genotypes and vertical lines separate individual samples. Images belonging to the same sample have the same number.

APPENDIX 3. PERIMETER LENGTH, CIRCULARITY AND DEPTH OF THE CELLULARIZATION FRONT PER TIME

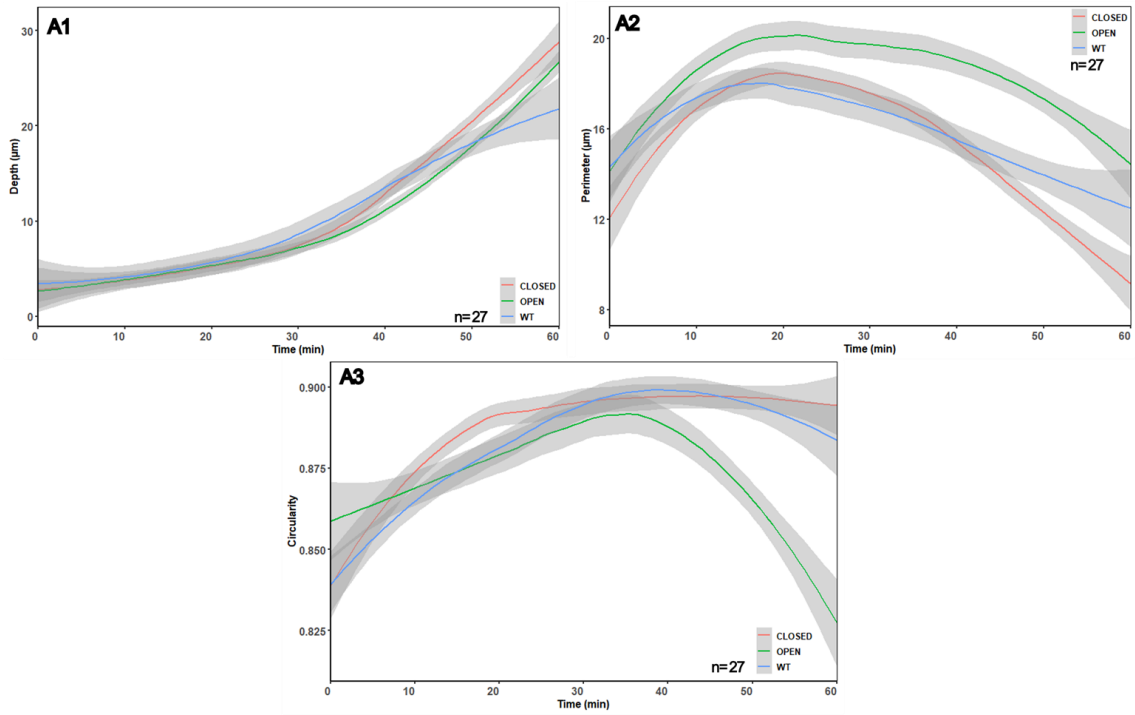

Figure 2: Difference in the perimeter length per time and circularity per time of the filamin rings as well as the depth per time of the cellularization front between the genotypes. The colored lines represent the average filamin ring perimeter length (µm) in A1, the average filamin ring circularity in A2 and the average front depth (µm) in A3. In A1-3 the red color represents CLOSED genotype (n=10), green OPEN genotype (n=7) and blue WT genotype (n=10). Standard error is represented as the gray area around the average line.